Research on Engineering Structures & Materials
www.jresm.org
MIM Research Group

Research Article

Shear behavior of RC beams without stirrups made of concrete core and external prefabricated U-shaped UHPFRC plates

Mohammed A. Sakr [a], Emad Etman [b], Tarek M. Khalifa [c], Esam A. Darwish [d], Mohamed Ali [*,e]

Structural Engineering Department, college of Engineering, Tanta University, Tanta, Egypt

Article Info

Article History:

Received 25 Oct 2025

Accepted 23 Nov 2025

Keywords:

Shear behavior,
Ultra-High-performance fiber-reinforced concrete,
RC beams,
Without stirrups,
Normal weight concrete,
Cellular lightweight concrete

Abstract

This study investigates the shear behavior of innovative T-shaped composite reinforced concrete (RC) beams without stirrups. The novelty of this study lies in investigating the shear behavior of stirrup-free, T-shaped composite beams that use an encased UHPFRC plate configuration as integrated permanent formwork. Six T-beams were tested: one RC reference beam and five composite beams with 30mm thick UHPFRC plates. Variables included interfacial properties (smooth, rough, anchored) and plate configurations (terminating at flange bottom or embedded within). One beam used cellular lightweight concrete (CLC) blocks to assess core concrete type. Four-point loading tests revealed that the UHPFRC plates significantly enhanced structural performance, increasing shear strength by up to 110.4% and deformation capacity 381.3% compared to a conventional RC beam. Critically, embedding the UHPFRC plates into the concrete flange with a rough interface proved to be the most effective configuration. This approach transformed the failure mode from brittle shear to ductile flexure and prevented premature debonding. This composite system presents a promising approach for enhancing the structural performance and durability of RC beams.

1. Introduction

Concrete has been a cornerstone of construction for centuries and remains one of the most widely used materials globally, with an estimated annual consumption of approximately 11 billion tons [1]. Apart from water, no other material is consumed in greater quantities. Today, the construction industry faces a critical challenge: reducing its environmental impact while fostering the development of sustainable building practices. Enhancing the sustainability of reinforced concrete (RC) structures can be achieved by extending their service life in both new and existing applications. Ultra-high-performance fiber-reinforced concrete (UHPFRC) is particularly suited for this purpose due to its exceptional properties, including high tensile and compressive strength, superior durability, and excellent ductility. These qualities make it a dependable option for enhancing structural durability and robustness. The exceptional properties of UHPFRC are derived from its densely compact matrix, characterized by minimal porosity, and its reinforcement with steel microfibers. These features offer significant advantages over Concrete with normal weight (NWC) and Concrete with light weight (LWC). However, the high cost of producing UHPFRC—both economically and environmentally—limit its feasibility for large-scale applications, posing a challenge to its widespread adoption [2–5].

To address these limitations while leveraging the benefits of UHPFRC, this study proposes an innovative composite system. The approach strategically confines the UHPFRC to a thin, prefabricated U-shaped outer shell that acts as permanent formwork for a more economical core

*Corresponding author: PG_69912@f-eng.tanta.edu.eg
[a]orcid.org/0000-0003-2863-3574; [b]orcid.org/0000-0002-2866-9537; [c]orcid.org/0009-0009-6511-1098;
[d]orcid.org/ 0000-0002-4861-2896; [e]orcid.org/ 0000-0001-9131-7561
DOI: http://dx.doi.org/10.17515/resm2025-1296me1025rs

material, such as normal weight concrete (NWC) or lightweight concrete (LWC). This method not only minimizes the required volume of costly UHPFRC but also utilizes its superior properties to enhance the overall structural performance and durability of the beams. These composite beams offer several advantages, including simplifying construction, reducing structural dead weight, and enabling longer spans or shallower beam depths. They also exhibit significantly higher shear capacity and ductility compared to conventional RC beams of the same dimensions.

Previous research has examined the UHPFRC-NWC interface, focusing on factors like surface roughness and the use of lightweight concrete cores to reduce dead weight [7-16]. However, these studies have also highlighted a critical issue: the separation of the outer UHPFRC layer from the concrete core, particularly when using lower-strength concrete. This debonding can limit the ultimate capacity and prevent the system from achieving its full potential.

While previous research has successfully explored UHPFRC shells for rectangular composite beams, the behavior of T-shaped sections without shear stirrups—a common configuration in practice—remains under-investigated. The complex geometry of T-beams introduces a critical challenge at the web-flange junction, where stress concentrations can lead to premature debonding of the UHPFRC shell from the concrete core. Furthermore, the effectiveness of fully encasing the UHPFRC plates within the flange to prevent this delamination has not been thoroughly examined. This study directly addresses these gaps by asking the following scientific questions: (1) How does the UHPFRC-NWC interface condition (smooth, rough, anchored) affect shear capacity and failure mode? and (2) Can embedding the UHPFRC shell into the flange transform the failure from brittle shear to ductile flexure by preventing interface delamination?

2. Material Properties

2.1. Ultra-High-Performance Fiber-Reinforced Concrete (UHPFRC)

In this study, the UHPFRC material's homogeneity and density were enhanced by exclusively using fine particles. To make a well-balanced mixture, dry silica fume, quartz, and cement were combined with sand that had a maximum particle size of 500 μm. To keep the mixture workable, Sika viscocrete superplasticizer (S.P.) and a low water/cement ratio were also used. Steel fibers with end hooks, comprising 2% of the mixture by volume, were added. These fibers had lengths of 13 mm and 20 mm and a fine diameter of 0.2 mm (see Fig. 1).

(a) (b)

Fig. 1. Steel fibers used in UHPFRC mixture: (a) hooked steel fiber (13 mm); (b) hooked steel fiber (20 mm)

They possess an impressive tensile strength of 2850 MPa and high elasticity modulus of 200 GPa, making them highly effective for reinforcing the matrix and enhancing its mechanical properties. Type I Portland cement (52.5 R) was chosen for the mixture. The ingredients are detailed in Table 1. The material preparation involved a stepwise mixing process: After four minutes of mixing all the dry materials, water and superplasticizer were gradually added. The addition of steel fibers occurred once the mixture achieved a uniform wet consistency. The specimens were cast, demolded 48 hours later, and then cured for 26 days in a water tank. Twenty-eight days after casting, the specimens were tested. To determine the flexural properties of the UHPFRC, three

prism specimens measuring 40 × 40 × 160 mm^3 were tested according to ASTM C1609/C1609M-19a - Standard Test Method for Flexural Performance of Fiber-Reinforced Concrete (Using Beam with Third-Point Loading) [26].

Table 1.Mix proportion of UHPFRC

Unit weight (kg/m^3)							
Cement	Sand	Quartz	Silica fume	Water	Superplasticizer (S.P)	Steel fiber (13 mm)	Steel fiber (20 mm)
850	1005	250	150	180	55	112	45

The prisms were simply supported over a clear span of 120 mm and subjected to load through two rollers spaced 40 mm apart. A constant displacement rate of 0.1 mm/min was applied until failure. This standard recommends these dimensions for testing fiber-reinforced concrete, and the chosen size ensures that the smallest cross-sectional dimension (40 mm) is more than twice the length of the longest steel fibers (20 mm), thus minimizing potential size effects on the measured flexural properties (ACI Committee 544, 2018) [29]. Compression tests were subsequently performed on three 150 × 150 × 150 mm^3 cube specimens following BS EN 12390-3:2019 - Testing hardened concrete — Part 3: Compressive strength of test specimens [27]. While this European standard is specifically for cube specimens, the testing procedure also generally adhered to the principles outlined in ASTM C39/C39M-21 - Standard Test Method for Compressive Strength of Cylindrical Concrete Specimens [28]. In this research, a universal testing equipment with a 500 kN capacity was used to conduct tests. The results of the compression and flexural testing are summarized in Table 2.

Table 2. Properties of UHPFRC

Material	Compression strength (MPa) at 28 days	Poisson's ratio	Elastic modulus (MPa)*104	Tensile strength,f_{ct} (MPa)	Flexural strength (MPa)
UHPFRC	115 ± 1.8	0.22	4.7 ± 0.3	7.4 ± 0.4	20 ± 0.5

Note: compressive strength, tensile strength and flexural strength are mean value of experimental ones.

To investigate the direct tensile stress-strain behavior of the UHPFRC, three custom-cast, dog-bone shaped specimens were prepared. The specimen geometry and testing methodology were designed following the recommendations of RILEM TC 162-TDF [30]. This was done to ensure a state of pure uniaxial tension and prevent premature failure at the grips. The specimens had a central prismatic section of 100 × 100 mm^2 where elongation was measured. These samples were created using the same mixture that was used to create the prefabricated UHPFRC plates for the composite beam manufacturing. The tests were performed under uniaxial tension using a 300 kN capacity universal testing machine. The specimens were secured using wedge-type mechanical grips designed to ensure failure occurred in the central gauge section. The load was applied monotonically at a displacement rate of 0.5 mm/min until failure. To accurately capture the tensile strain, two Linear Variable Differential Transformers (LVDTs) were mounted on opposite faces of the specimen over a gauge length of 100 mm. The nominal tensile stress was computed by dividing the measured load by the initial cross-sectional area of the specimen's central section (100 × 100 mm^2), while the strain was determined by dividing the measured elongation by the original gauge length. All measuring instruments, including the load cell and LVDTs, were calibrated according to manufacturer specifications prior to the testing program. Fig. 2 shows the average uniaxial tensile stress-strain behavior of the UHPFRC. The average tensile strength was 7.4 MPa, with a standard deviation of 0.4 MPa. The average strain at peak stress was 0.01, with a standard deviation of 0.0008. The UHPFRC exhibited a linear elastic response up to approximately 7.4 MPa, followed by gradual softening. The tensile rupture strain was slightly above 0.01, as illustrated in Fig. 2.

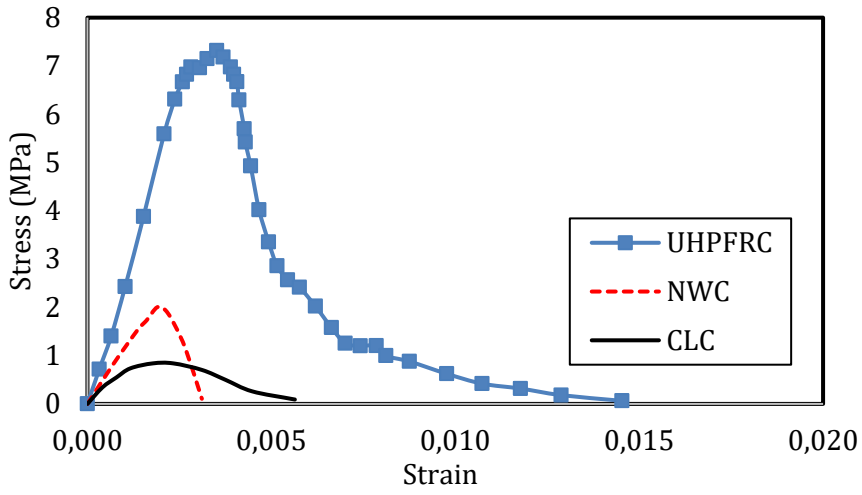

Fig. 2. Uniaxial tensile behavior of CLC, NWC and UHPFRC

2.2. Normal Weight Concrete (NWC)

Concrete with a target compressive strength of 30 MPa was used for the cores of the composite beams. The mix consisted of ordinary Portland cement (Type I), coarse aggregate with a maximum size of 10 mm, fine aggregate, and water. The proportions and characteristics of the concrete mix are summarized in Tables 3 and 4.

Table 3. Mix proportion of normal weight concrete

water-to-cement ratio. (w/c) %	Unit weight (kg/m3)			
	Water	Cement	Fine aggregate	Coarse aggregate (≤ 10 mm)
50	190	380	660	1173

Table 4. Properties of NWC and CLC

Material	Density (kg/m^3)	Compressive strength (MPa)	Elastic modulus (MPa)*104	Tensile strength,f_{ct} (MPa)	Poisson's ratio
NWC	2500	32 ± 0.8	2.45 ± 0.2	2.0 ± 0.3	0.20
CLC	700	2.12 ± 0.15	0.21 ± 0.02	0.47 ± 0.06	0.25

Note: compressive strength, tensile strength and elastic modulus are mean value of experimental ones

To determine the compressive strength of the NWC, three 150 × 150 × 150 mm^3 cube specimens were tested according to BS EN 12390-3:2019 [27]. The testing procedure also generally adhered to the principles outlined in ASTM C39/C39M-21 [28]. The tests were performed using a universal testing machine with a capacity of 500 kN. The load was applied monotonically at a rate of 0.6 MPa/s until failure. This loading rate is within the range specified by BS EN 12390-3:2019 [27]. The average compressive strength of the NWC at 28 days was determined to be 32 MPa, with a standard deviation of 0.8 MPa (Table 4). To characterize the tensile behavior of the NWC, direct tension tests were performed on three dog-bone shaped specimens prepared from the same concrete batch as the beam cores. The testing procedure was consistent with that used for the UHPFRC specimens, guided by the principles of RILEM TC 162-TDF [30]. The tests were conducted using the same universal testing machine and instrumentation setup, and the specimens were secured with wedge-type mechanical grips. The load was applied monotonically at a constant displacement rate of 0.5 mm/min until failure. Elongation was measured over a gauge length of 100 mm using two LVDTs. As with the UHPFRC tests, the nominal tensile stress was calculated by dividing the measured load by the initial cross-sectional area, and the equipment was calibrated prior to use. Fig. 2 shows the average uniaxial tensile stress-strain curve for the NWC. The average tensile

strength was 2.0 MPa, with a standard deviation of 0.3 MPa. The average strain at peak stress was 0.003, with a standard deviation of 0.0004. The NWC exhibited a linear elastic response up to approximately 2.0 MPa, followed by softening, with a tensile rupture strain of approximately 0.003.

2.3. Cellular Lightweight Concrete (CLC) Blocks

For one of the beams, the core utilized cellular lightweight concrete (CLC) blocks supplied by the Delta Mix factory. According to the author's previous research [18], the properties of the CLC blocks are detailed in Table 4, providing key insights into their mechanical and physical characteristics. Additionally, Fig. 2 illustrates the direct tensile stress–strain behavior of the CLC material, highlighting its performance under tensile loads.

2.4. Steel Reinforcement

The beams were reinforced with deformed steel bars having diameters of 16 mm, 12 mm, and 10 mm for the longitudinal reinforcement. The concrete slab's ribbed bars were arranged in two layers: 155 mm center-to-center (10 mm in diameter) horizontally and 196 mm center-to-center (8 mm in diameter) vertically. It is crucial to note that these beams are designed to be 'without stirrups' in the shear spans. A minimal number of four 6 mm-diameter stirrups were installed only at the loading and support points, outside the critical shear regions. Their sole purpose was to maintain the geometry of the reinforcement cage during casting and they did not contribute to the shear capacity of the beams. The universal testing equipment conducted tension tests on the reinforcing steel bars to determine their yield and ultimate strengths. The tensile characteristics of the longitudinal reinforcement used in this research are detailed in Table 5.

Table 5. Measured properties of longitudinal reinforcement

Diameter (mm)	Yield strength (MPa)	Ultimate strength (MPa)
Ø6, Ø8	243	352
Ø10, 12, 16	498	657

3. Experimental Program

3.1. Design of beams

Six T-beams in total were fabricated and tested, including one reinforced concrete (RC) beam as a reference and five beams utilizing prefabricated U-shaped UHPFRC as a permanent formwork with a thickness of 30 mm. These beams featured different interfacial properties: smooth (S), rough (R), and smooth with anchored shear connectors (SC). Additionally, two configurations were applied to the UHPFRC plates: one that stopped at the bottom of the concrete flange (Fig. 3a) and another that was encased directly into the concrete flange. In the encased configuration, composite action was achieved via transverse reinforcement bars passing through holes in the UHPFRC formwork (Fig. 3b). This created a robust mechanical connection. To assess the effect of core concrete type on shear behavior, one beam replaced normal weight concrete (NWC) with cellular lightweight concrete (CLC) blocks. The reference RC beam was labeled S0, and the composite beams were named according to their interfacial properties, such as S2-R for a composite beam with a rough interface. The beam using CLC blocks instead of NWC was designated S5-HB. T-shaped, simply supported beams with an effective span (L_0) of 1800 mm and a ratio of shear span-to-depth (λ) of 1.8. This specific shear span-to-depth ratio (λ=1.8) was selected to ensure the specimens behave as deep beams, where the load transfer mechanism is dominated by arch action rather than beam action. This represents a critical condition for shear behavior in discontinuous regions where stirrups are often omitted or difficult to detail [35]. The lower part width (b) of 150 mm, a concrete slab width (B) of 500 mm, a slab thickness (tb) of 100 mm, and a U-shaped UHPFRC plate thickness (tw) of 30 mm were used for all specimens. The concrete slab's ribbed reinforcement had a 20 mm protective layer thickness, and the beam depth (H) was 350 mm. For longitudinal reinforcement on the tension side, all beams, except for the S5-HB beam, were reinforced with two bars with 16 mm diameter and two bars with 12 mm diameter in the NWC core.

(a) (b)

Fig. 3. Cross section of the composite beam with NWC core and UHPFRC cover, showing two plate configurations: (a) plate terminating at the bottom of the flange; (b) plate encased directly into the flange

The S5-HB beam, however, utilized four 12 mm diameter bars and two 10 mm diameter bars in the soffit of the UHPFRC plate. Two bars of 10 mm diameter compression steel were attached to the top of all beams. For the concrete slab, two layers of ribbed bars were utilized, spaced 155 mm center-to-center (10 mm in diameter) horizontally and 196 mm center-to-center (8 mm in diameter) vertically. Finally, simultaneous casting was used to integrate the slab with the concrete inside the prefabricated U-shaped UHPFRC plate. Fig. 4 provides the dimensional details of all beams, while Table 6 lists the specific details of each specimen.

Table 6. Summary of beams

Beam	Matrix	Interfacial properties	tb (mm)	Length (mm)	Width (mm)	Depth (mm)	Longitudinal bars	
							As (mm^2)	μ (%)
S0	NWC	--	100	2000	150	350	628	1.2
S1-R	UHPFRC-NWC	Rough						
S2-R	UHPFRC-NWC	Rough						
S3-S	UHPFRC-NWC	Smooth						
S4-SC	UHPFRC-NWC	Smooth with connectors						
S5-HB	UHPFRC-CLC	Smooth					609	1.2

Note: -- means no data, μ represents the longitudinal tensile reinforcement ratio.

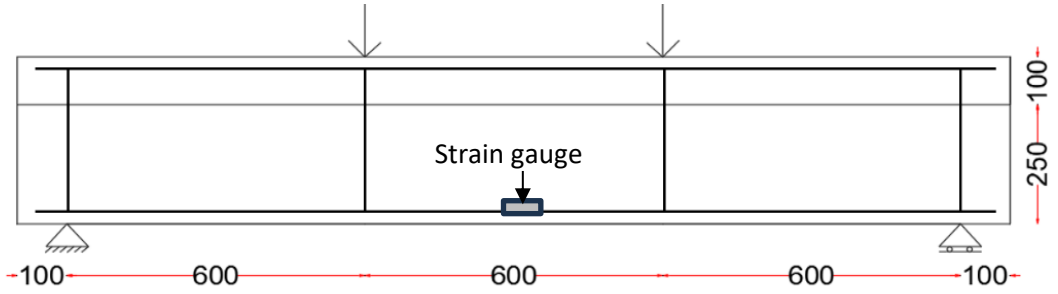

Fig. 4. Dimensions details of all beams

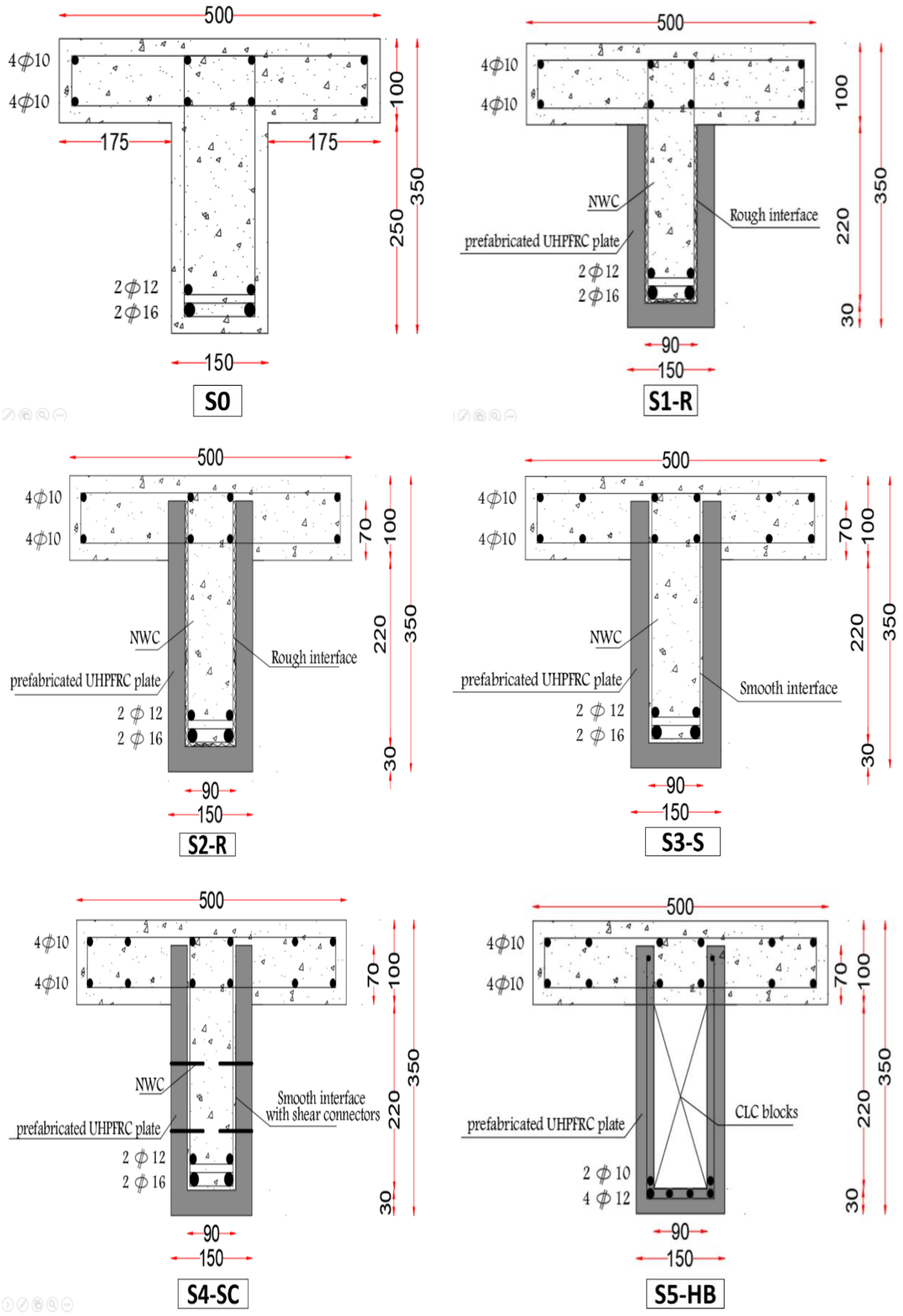

Fig. 5. Cross section and reinforcements of all beams

To monitor the yielding of the reinforcing bars, a strain gauge was attached to the center of the bars on the tension side. The configuration of the beams and the reinforcement positioning within the

concrete and UHPFRC components are clearly depicted by the cross-section and reinforcement details for each beam in Fig. 5. Two rows of steel anchoring bars measuring 60 mm in length and 8 mm in diameter were inserted into the prefabricated U-shaped UHPFRC plate for the S4-SC beam, as shown in Fig. 6. These bars were spaced 86.5 mm apart in the longitudinal direction. The authors acknowledge that the limited number of six specimens restricts statistical generalization. However, the results provide clear and consistent trends for the investigated parameters.

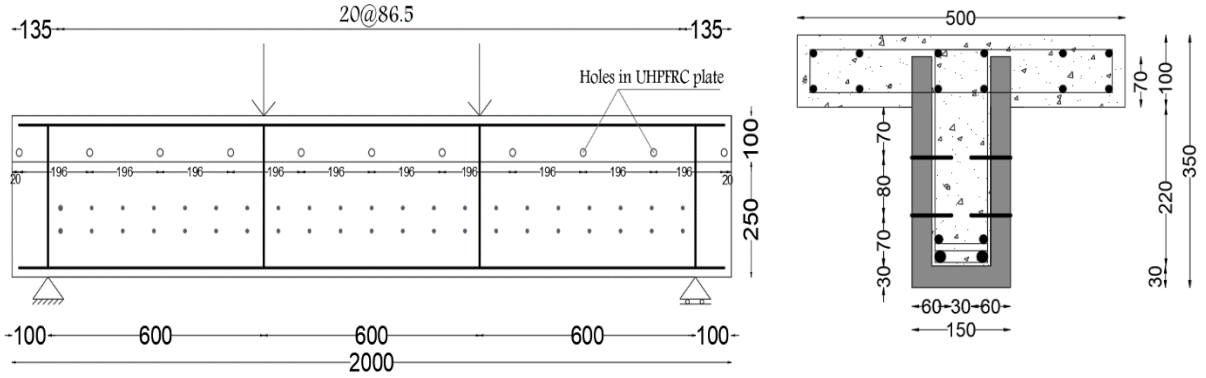

Fig. 6. Arrangement of anchorage steel bars in S4-SC beam

3.2. Beam Manufacturing

A UHPFRC plate thickness of 30 mm was selected as it provides sufficient cover for the steel microfibers, ensures robust handling during fabrication, and aligns with thicknesses used in similar prefabrication studies. The prefabricated U-shaped UHPFRC plates were precast utilizing an interior foamed plastic cubic and an exterior film-faced plywood formwork. The foamed plastic cuboid's surface could be changed to create various interfaces between the concrete and the UHPFRC plate. Three interface conditions were investigated: smooth, rough, and smooth with anchored shear connectors (SC). For the smooth interface (used in specimens S3-S), the UHPFRC was cast directly against the smooth surface of the foamed plastic cuboid.

This resulted in a surface with minimal texture and irregularities. For the rough interface (used in specimens S1-R and S2-R), the surface of the foamed plastic cuboid was mechanically abraded prior to casting the UHPFRC. This abrasion was performed using a wire brush, to create a surface with noticeable indentations and protrusions. The resulting rough interface was characterized by a highly irregular surface with numerous small indentations and protrusions, and a coarse, abrasive texture (see Fig. 7). It is acknowledged that this characterization is qualitative, and future work should incorporate quantitative roughness measurements (e.g., laser profilometry to determine metrics like Ra or Rz) to establish a more precise correlation between interface topography and structural performance.

(a)

(b)

(c)

(d)

Fig. 7. Prefabricated U-shaped UHPFRC plates with different interfacial properties: (a) smooth interface; (b) rough interface; (c) smooth interface with shear connectors; (d) CLC blocks used for formwork

For the smooth interface with anchored shear connectors (used in S4-SC beam), a cuboid with steel anchoring bars evenly spaced was employed to create a smooth interface with these bars as shown in Fig. 8. In contrast, the S5-HB beam replaced the foamed plastic cuboid with CLC blocks, and the longitudinal reinforcement is moved to the external prefabricated UHPFRC plate. The process began with the setup of the external film-faced plywood formwork, followed by the placement of the foamed plastic cuboid inside to form a U-shaped cavity. Fresh UHPFRC was then poured into the cavity from the bottom to the top. Fresh UHPFRC was then poured into the cavity, filling it completely from the bottom upwards.

Fig. 8. Prepared inner and external formwork for S4-SC beam

Fig. 9. Prepared inner and external formwork for all beams

Fig. 9 illustrates the external and internal formwork used for all the beams. The formwork was removed one day after casting. Fig. 7 shows the prefabricated U-shaped UHPFRC plates with various interfacial characteristics. Both ends of the prefabricated U-shaped UHPFRC plates were covered with film-faced plywood plates to provide a sealed cavity for the concrete before the steel cage and reinforcement for the concrete slab flange were installed. Once the formwork was secured, the steel cages and slab reinforcement were positioned at the designated locations within the prefabricated U-shaped UHPFRC plates and the flange plywood formwork, respectively. The casting process was then finished by pouring concrete into the prefabricated UHPFRC plate formwork. After 24 hours, the plywood plates at both ends and the flange formwork were removed. The U-shaped UHPFRC formwork and concrete were cast simultaneously. The beams were wrapped in sheets of plastic and sprayed with water every day for at least 28 days to guarantee adequate curing. The process flow for fabricating composite beams is shown in Figs. 10(a-h).

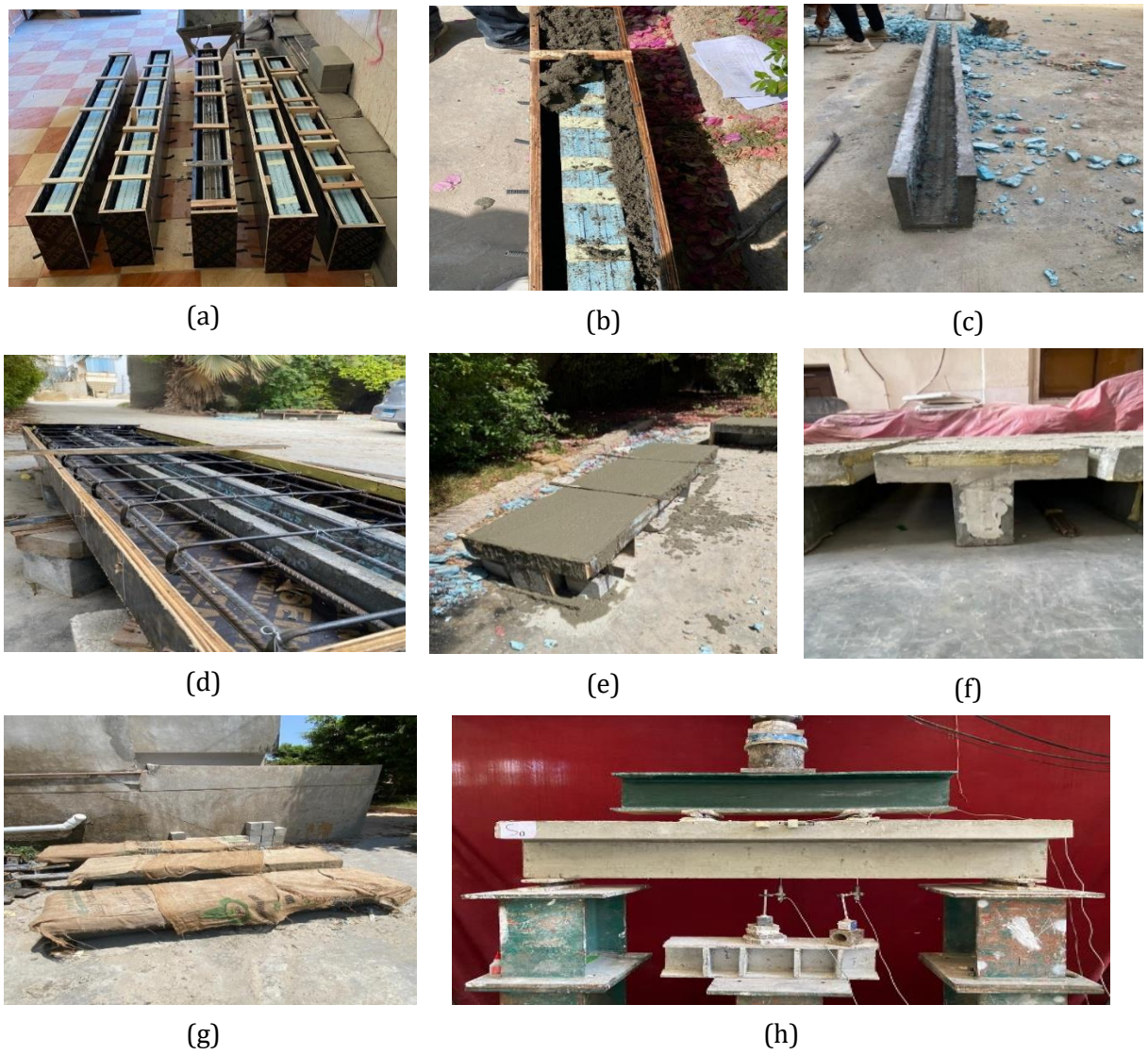

Fig. 10. Flow chart of the composite beam fabrication process: (a) preparing formwork; (b) casting UHPFRC plates; (c) demolishing formwork; (d) setting up steel reinforcement; (e) casting concrete core and flange; (f) demolishing flange formwork; (g) curing; (h) testing

3.3. Experimental Test

A 4-point load test was applied to all the beams, with the two loading points spaced 600 mm apart. To monitor the mid-span deflection, two LVDTs were employed, while another LVDT was used to measure the compression strain in the concrete flange. To monitor strain on each beam's side of tension, a strain gauge was attached to the center of just one longitudinal bar. The load was applied in increments of 10 kN, with each step held for 10 seconds. This quasi-static procedure was chosen to allow for careful visual inspection, marking of crack initiation and propagation, and to ensure stable data acquisition before failure.

This methodology is consistent with established guidelines for structural load testing and is a common approach for experimental studies of this nature [37,38]. Crack widths were measured using a handheld optical microscope with a magnification of 40X and a precision of 0.02 mm. These measurements were recorded at the level of the longitudinal reinforcement after each 10 kN load increment. Additionally, the full crack pattern was mapped by tracing the cracks with a marker pen on the surface of the beams to document the failure evolution. All measuring instruments, including the LVDTs and the load cell, were calibrated prior to testing. The LVDTs were calibrated using a micrometer to ensure an accuracy of ±0.01 mm. The bearings for the load beneath the spreader beam were positioned across the entire width of the concrete flange, ensuring that the applied load

was shared by both the prefabricated U-shaped UHPFRC plates and the concrete beam. Fig. 11 represents the experimental setup.

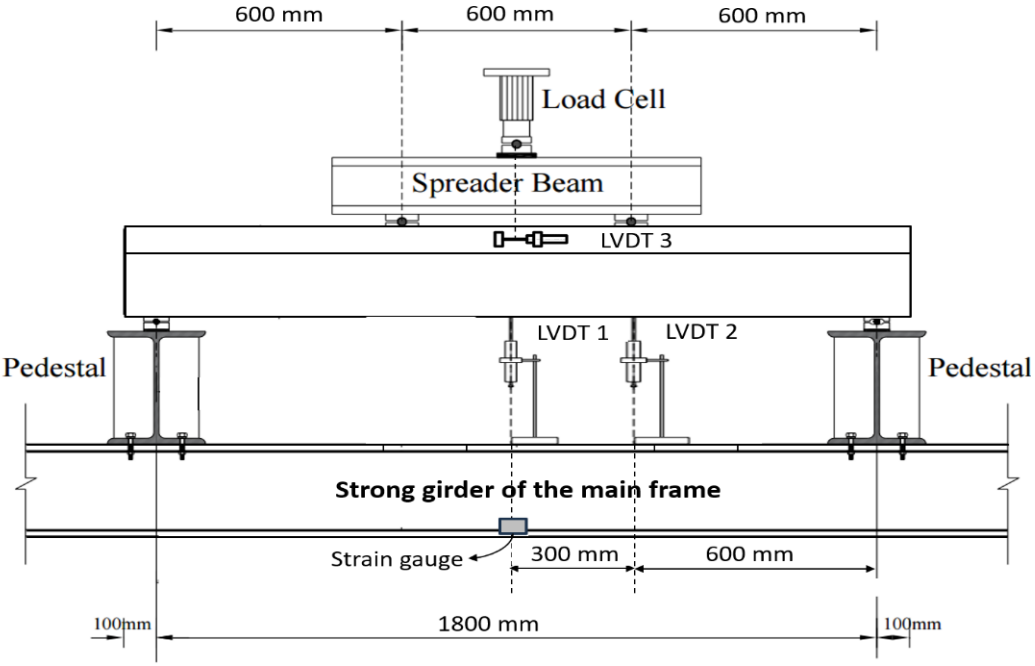

Fig. 11. Layout of the test setup

4. Results and Discussion

4.1. Cracking Patterns and Modes of Failure

Fig. 12 depicts the crack patterns that appeared in the beams when they reached their peak load capacity. It is noteworthy that a large number of tiny cracks appeared in the prefabricated UHPFRC plates used in the composite beams. However, Fig. 12 only highlights the most significant cracks because of the short time available for crack monitoring during the loading testing. In all tested beams, flexural cracks first appeared in the area that was subjected to pure bending. More cracks formed throughout the shear spans as the load increased. In the reference beam S0, the load-carrying capacity dropped sharply, accompanied by a fracture sound, when an inclined crack formed through the shear span (see Fig. 12a). The remaining composite beams, on the other hand, failed considerably more gently and showed higher ductility. In contrast to the other composite beams, the S3-S composite beam experienced less inclined cracks with (see Fig. 12d). This suggests that the prefabricated U-shaped UHPFRC plate with a smooth interface in beam S3-S was less effective in working cooperatively with the concrete to carry the load because of weaker properties of the interfacial layer. More than two inclined cracks appeared in all composite beams, although the reference beam S0 only had one (see Fig. 12a). Significant separation at the interface beneath the flange occurred at peak load in the S1-R beam, as seen in Fig. 12b, while no separation was observed in the other composite beams. This indicates that encasing the UHPFRC plates directly into the concrete flange was highly effective. The transverse reinforcement bars passing through holes in the plates securely anchored the two materials, preventing any separation at the interface. The midpoint stress in the longitudinal bars of all beams (except S0 and S5-HB) reached yield. This suggests that the use of prefabricated U-shaped UHPFRC plates transformed the brittle shear failure into a more ductile failure. All beams failed due to shear, except for beam S2-R, which experienced ductile flexural failure. As shown in Fig. 12c, failure of the UHPFRC plates in S2-R beam occurred when the beam reached its full capacity. In the pure bending zone, vertical cracks were observed and in the shear span, inclined cracks formed. As a result, every material in the S2-R beam was used.

(a)

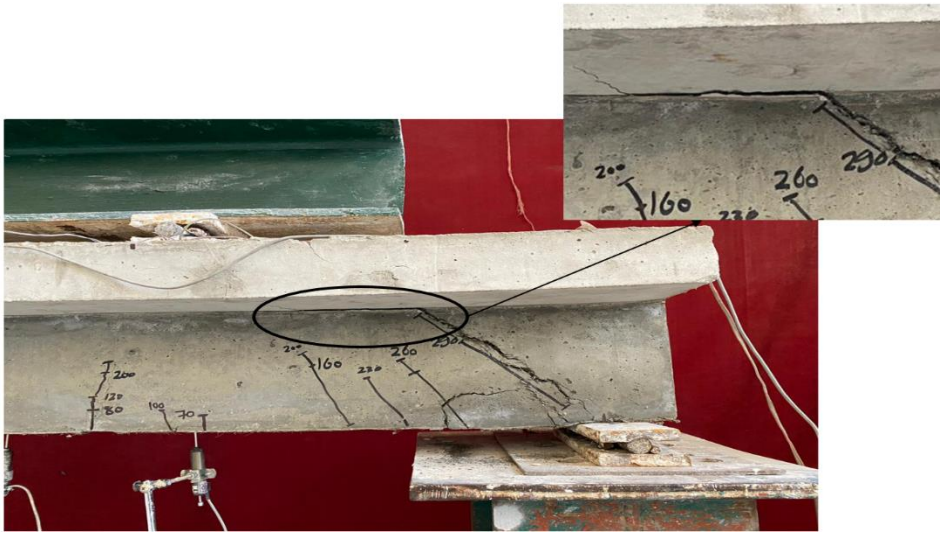

(b)

(c)

(d)

(e)

Fig. 12. Crack patterns at peak load for beams: (a) reference beam S0; (b) beam S1-R, showing interface separation; (c) beam S2-R; (d) beam S3-S; (e) beam S5-HB

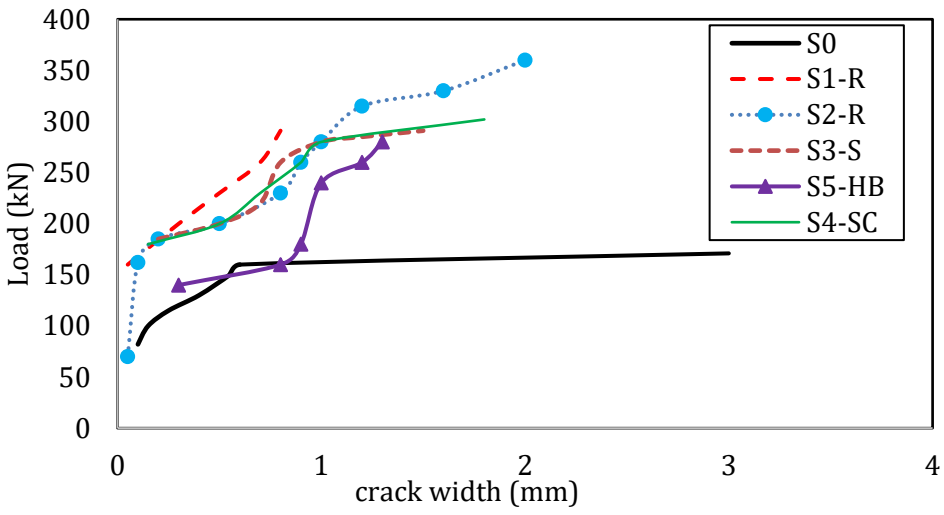

Fig. 13. Load versus major crack width for all tested beams

To provide a quantitative analysis of the cracking behavior, the width of the primary diagonal shear crack in each beam's shear span was measured and plotted against the applied load, as shown in Fig. 13. This figure clearly illustrates the fundamental difference in failure mechanics between the reference beam and the composite specimens. The reference beam (S0) exhibited a sharp increase in crack width after its formation, reaching over 2.5 mm at its peak load of approximately 171 kN. This behavior, characterized by the steep, short curve in Fig. 13, is indicative of poor crack control and confirms the brittle nature of its shear failure. In stark contrast, all composite beams demonstrated significantly improved crack control. For instance, at the same load level of 171 kN where S0 failed, the major crack width in the superior S2-R beam was only around 0.2 mm. The S2-R beam continued to sustain load up to 360.5 kN, with its crack opening in a slow and controlled manner. This highlights the effectiveness of the UHPFRC plates, particularly the embedded configuration (S2-R), in bridging cracks and ensuring a more ductile response by allowing for gradual stress redistribution. The behavior of the other composite beams also shows a marked improvement over the reference, though debonding in S1-R led to a slightly faster crack opening compared to the other composite beams before failure. These quantitative data strongly support the conclusion that the UHPFRC plates transform the failure mode from brittle shear to a more ductile mechanism governed by controlled crack growth.

4.2. Load-Deflection Graphs

Fig. 14 depicts the correlation between mid-span deflection and applied load for all beams. The mid-span deflection values were obtained from the LVDT placed at the beam's midpoint. All of the composite beams' peak loads were noticeably greater than those of the reference beam S0, attributed to the enhanced ductility of the UHPFRC. Additionally, all composite beam's stiffness exceeded that of S0 after the first crack, confirming that the fiber-bridging action helps UHPFRC structural members keep stiffness better than RC members.

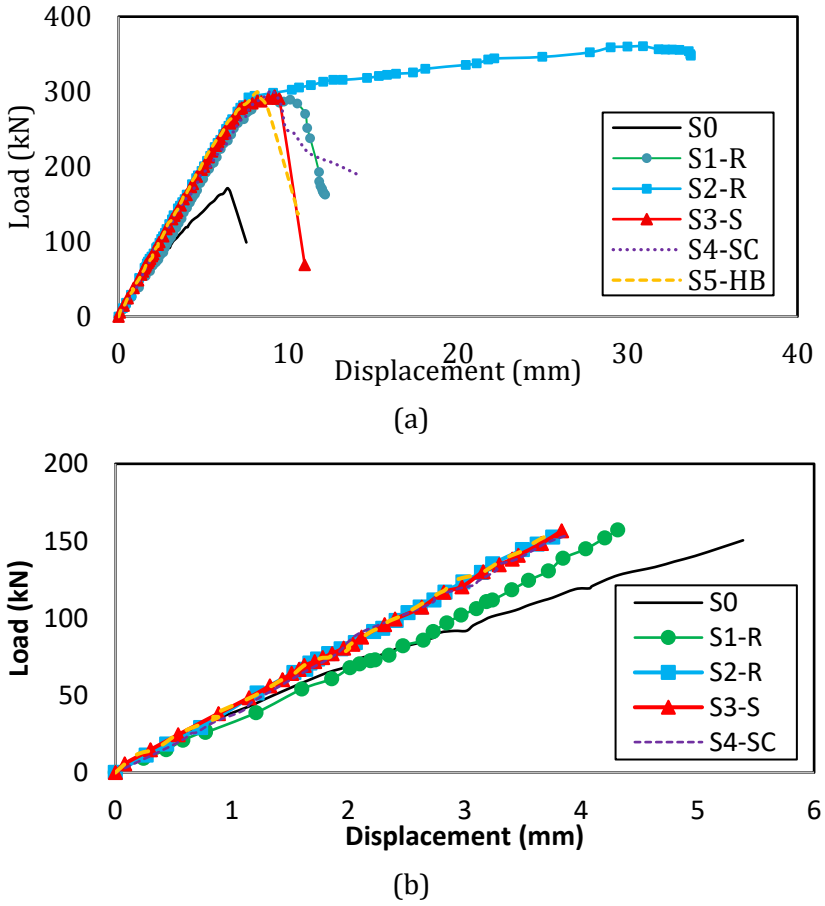

Fig. 14. Load vs. mid-span deflection curves for all tested beams: (a) the full response, showing ultimate capacity and overall ductility, and (b) a zoomed-in view of the initial load region, highlighting the differences in stiffness

Table 7 summarizes the key experimental results. Specimens S3-S, S4-SC and S5-HB exhibited comparable behavior. Specimen S3-S serves as the reference for describing the sequence of stages for load-deflection curve which divided into elastic, elastic-plastic, and descending stages. Together, the prefabricated UHPFRC plate, and encased concrete withstand shear forces that are transmitted from the loading point to the supports during the elastic stage, with load and mid-span deflection increasing linearly. In the middle of the span, at the bottom of the beam, the first vertical flexural crack developed at a load of 65 kN, indicated the transition to the elastic-plastic stage. During this stage, stiffness decreased continuously. The diagonal cracks started during the elastic-plastic phase and progressively propagated across the depth of the prefabricated UHPFRC plate. The encased concrete's contribution to shear capacity decreased once it reached its maximum shear strength, and more shear force was resisted by the prefabricated UHPFRC plate. The longitudinal reinforcement yielded at a load of 237 kN. The prefabricated UHPFRC plate's plastification stopped when a diagonal crack developed, and the crack became approached its compressive strength. With a mid-span deflection of 9.19 mm (L0/196), the specimen reached its maximum load of 294.5 kN. Following this, the load dropped sharply due to diagonal crack crushing, as depicted in Fig. 12d. The separation between the core concrete and UHPFRC plate in previous studies [10,11] were prevented by the UHPFRC plate's upper straight sides, which were directly encased in the concrete flange. This improved the integrity of the beam and behaved as a composite beam as it was designed.

Table 7. Summary of experimental results for All Beams

Beam ID	Pcr (kN)	Py (kN)	Pu (kN)	Gain in shear capacity (%)	Mid-span deflection at peak load (Δ) (mm)	Gain in deformation capacity (%)	Failure mode
S0	50	--	171.36	--	6.42	--	Shear failure
S1-R	65	--	291.72	70.23	9.36	45.8	Shear failure
S2-R	70	274	360.57	110.41	30.90	381.3	flexure failure
S3-S	65	237	294.78	72.02	9.19	43.1	Shear failure
S4-SC	66	238	301.92	76.19	9.02	40.5	Shear failure
S5-HB	40	--	299.88	75.0	8.18	27.4	Shear failure

P_{cr} = Load at first visible crack; P_y = Load at yielding of longitudinal reinforcement; P_u = Ultimate load; -- indicates that the longitudinal reinforcement did not yield before failure. The percentage gain in shear capacity and deformation were calculated using the formula: Gain (%) = [(P_u or Δ_u, composite - P_u or Δ_u, S0) / P_u or Δ_u, S0] × 100.

Beam S1-R, featuring a rough interface and a UHPFRC plate terminating at the bottom of the concrete flange, exhibited a significantly different response compared to the reference beam, So. The first flexural crack was observed at a load of 65 kN, while the first shear crack appeared at a load of 160 kN (see Fig. 14 for crack pattern). As the load increased, multiple inclined shear cracks developed in the shear span, extending from the loading point towards the support. The load-deflection curve (Fig. 13) showed an initially linear response, followed by a gradual decrease in stiffness as cracking progressed. A significant observation for beam S1-R was the initiation of progressive debonding at the UHPFRC-concrete interface beneath the flange as it approached its peak load of 291.72 kN. This separation, highlighted in Fig. 12c is a classic debonding failure. This can be explained by shear-friction theory, where the horizontal shear stress at the NWC-UHPFRC interface exceeded the shear resistance capacity. Without the mechanical anchorage provided by embedding the plate into the flange, the interface relied solely on adhesion and friction, which was insufficient to prevent slip and ultimately led to premature debonding. While the beam did not fail catastrophically, this debonding was the critical failure mechanism limiting its ultimate capacity. The stiffness retained after debonding began does not reflect a full bond. Instead, it is attributed to residual friction and partial aggregate interlock at the interface, which allowed for limited shear transfer until failure. The strain gauge on the longitudinal reinforcement did not reach the yield strain (2500 με) at peak load, indicating that the beam failed in shear before the reinforcement yielded. The final failure mode was characterized as a brittle shear failure with significant interface

debonding. The peak load was 70.23% higher, and the deformation was 45.79% than the reference beam So.

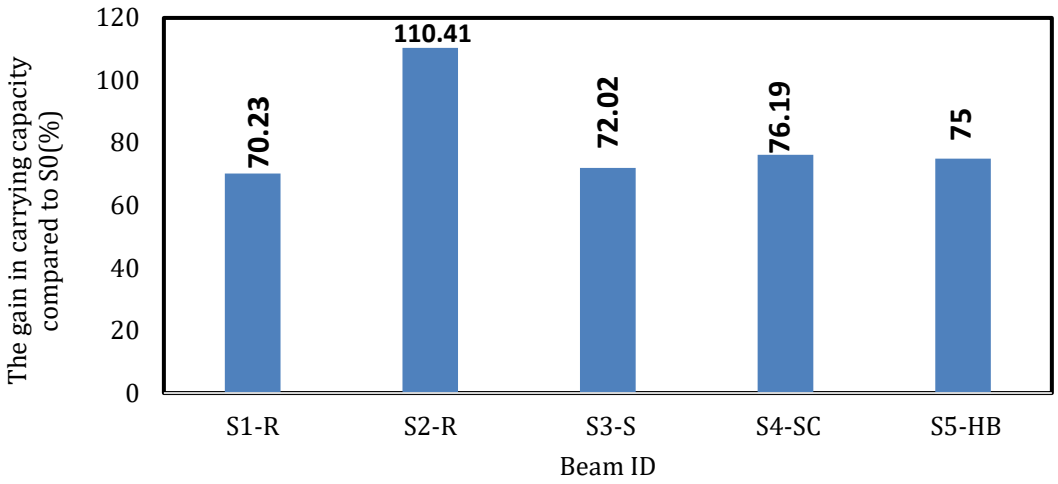

(a)

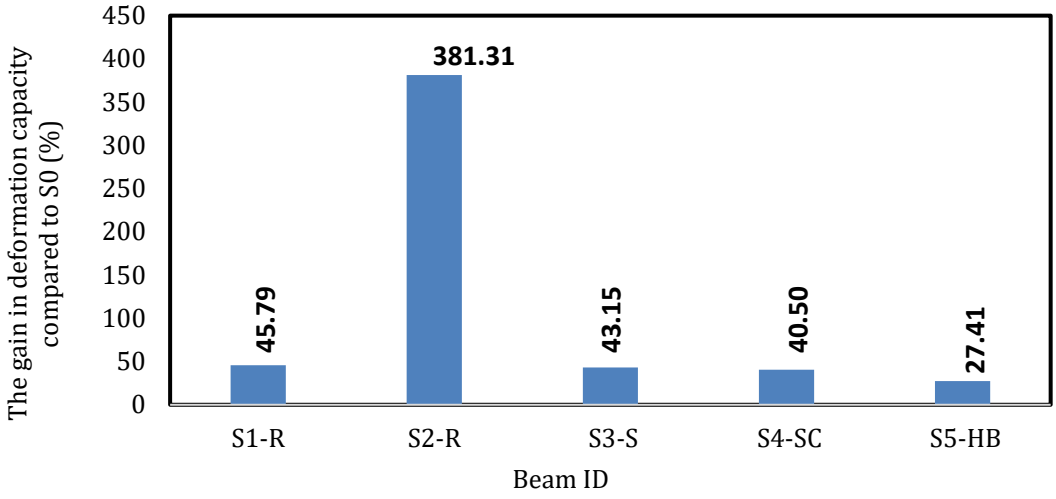

(b)

Fig. 15. Percentage gain in capacity compared to the reference beam S0: (a) carrying capacities; (b) deformation capacities

Specimen S2-R exhibited the largest mid-span deflection corresponding to the peak loads compared to the other composite beams due to its conversion from brittle shear failure to ductile flexural failure. The superior performance of S2-R is attributed to a combination of factors. The rough interface maximized the frictional and mechanical interlock, while embedding the plate into the flange provided a robust mechanical anchorage. This configuration effectively confined the concrete core, ensured composite action up to failure, and prevented the premature interface debonding seen in S1-R. The first flexural crack was observed at a load of 70 kN, followed by the first shear crack at 162 kN. As the load increased, multiple fine cracks developed within the UHPFRC plate in both the flexural and shear zones (see Fig. 12c). These cracks were more numerous and finer than those observed in the beams with terminating UHPFRC plates (e.g., S1-R). The load-deflection curve for Beam S2-R (Fig. 14) showed an initially linear response, followed by a gradual reduction in stiffness. Notably, this beam exhibited significant ductility after reaching its peak load of 360.57 kN. The strain gauge on the longitudinal reinforcement did reach the yield strain (2500 με) at a load close to the peak load (see Fig. 16a), indicating that the reinforcement yielded prior to failure. Furthermore, the concrete strain measurements near the loading point on the upper slab surface exceeded 3000 με (Fig. 16b), indicating crushing of the concrete in the

compression zone. Crucially, no separation was observed at the interface between the UHPFRC plate and the concrete core, even at peak load (see Fig. 12c). This contrasts sharply with the behavior of Beam S1-R, which exhibited significant interface debonding. The embedded configuration of the UHPFRC plate, combined with the rough interface, appears to have provided excellent composite action, preventing premature failure due to interface separation. The final failure mode of Beam S2-R was characterized as a ductile flexural failure, with yielding of the longitudinal reinforcement, crushing of the concrete in the compression zone, and extensive cracking of the UHPFRC plate. This indicates that all components of the composite beam (NWC core, UHPFRC plate, and steel reinforcement) were effectively utilized to resist the applied load. The peak load for Beam S2-R was 110.41% higher than that of the reference beam (So) and its mid-span deflection was 381.3% larger, demonstrating a significant improvement in both strength and ductility. For successful field applications of this optimal design, strict quality control is essential to ensure consistent interface roughness and proper placement of the transverse anchoring bars. The shear-carrying and deformation capacity of each beam are compared with the reference beam S0 in Fig. 15. The composite beams showed an increase in shear-carrying capacity by 70.2% to 110.4% and in deformation capacity by 27.4% to 381.3%, regardless of the prefabricated UHPFRC plate configuration, concrete core type, or properties of the interfacial layer.

4.3. Strain Analysis

Fig. 16 a and b represent the load-strain curves for the longitudinal reinforcement on the tension side and the concrete slab, respectively. The longitudinal reinforcement's strain was measured at the cross-section at the mid-span of the beam. In the beams S2-R, S3-S, and S4-SC, the longitudinal reinforcement on the tension side reached its yield strain of 2500 με prior to failure, with S2-R failing due to flexural failure and S3-S and S4-SC due to shear failure. This indicates that these beams effectively transformed the brittle shear failure into a more ductile failure mode which confirmed by the strain gauge data (Fig. 16a). The longitudinal reinforcement strain in beams S0, S1-R, and S5-HB remained well below yield, indicating a brittle shear failure occurred first. At the mid-span, concrete strain measurements were obtained from the slab's upper surface, close to the loading point. Near the loading plate, the concrete on the upper slab surface surpassed the 3000 με crushing strain in beams S0 that failed due to brittle shear failure and S2-R, suggesting that the materials in beam S2-R were fully utilized. Therefore, the UHPFRC plate configuration used in S2-R is recommended.

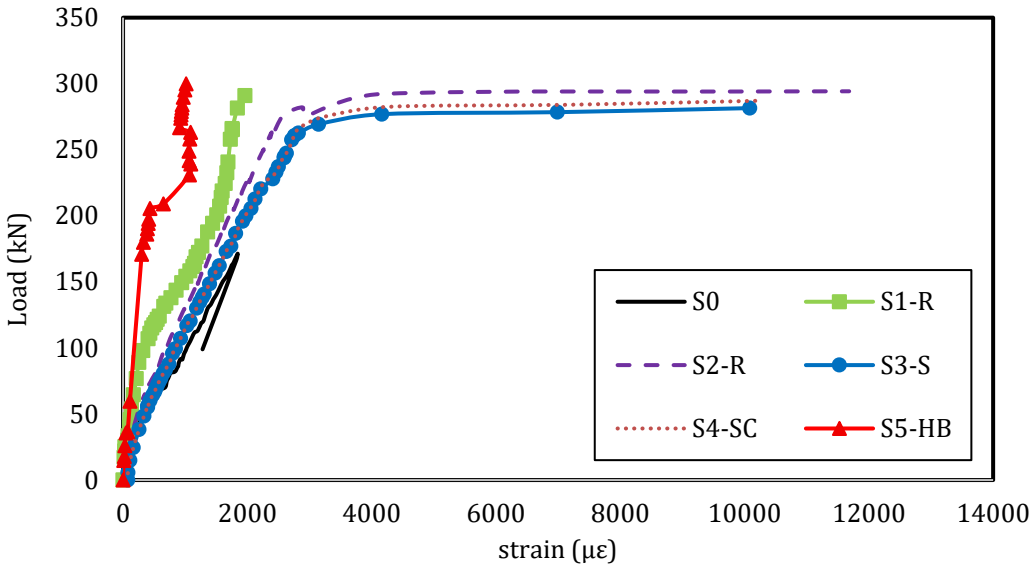

(a)

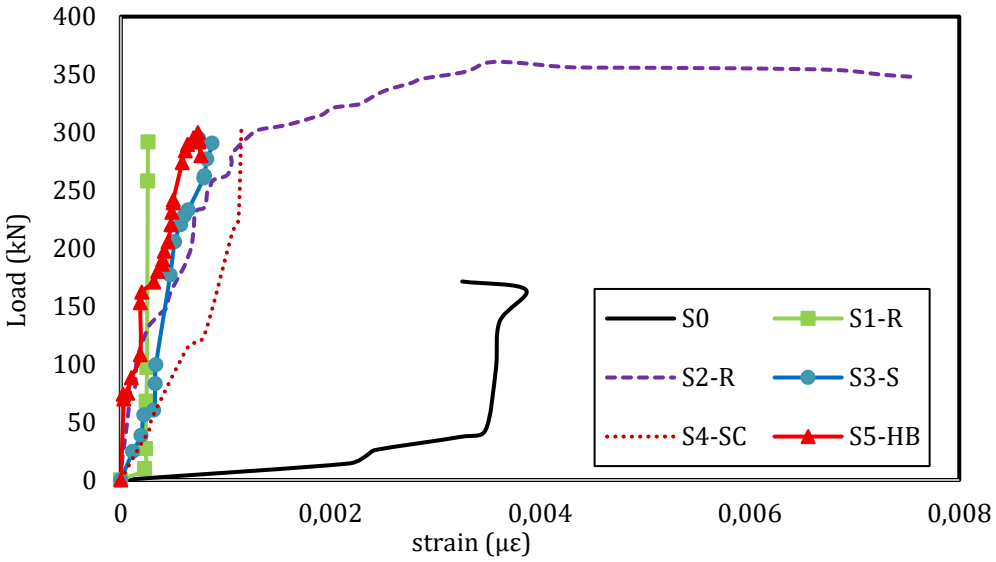

(b)

Fig. 16. Load-strain curves for concrete and steel reinforcement: (a) longitudinal reinforcement strain at mid-span; (b) concrete slab compressive strain near the loading point

4.4. Effects of the Prefabricated UHPFRC Plate Configuration

The effect of the prefabricated U-shaped UHPFRC plate configuration can be assessed by comparing the specimens' load vs mid-span deflection curves for S1-R and S2-R, as shown in Fig. 13. In the S1-R composite beam, the prefabricated UHPFRC plate was terminated at the bottom of the concrete flange (Fig. 3a), whereas in the S2-R composite beam, the plate was encased directly into the concrete flange. This encased configuration achieved composite action through perfect bond connections with reinforcement bars passing transversely through holes in the encased top sections of the UHPFRC plate (Fig. 3b). A significant detachment at the interface beneath the flange occurred at peak load in the S1-R beam, while no detachment was observed in the S2-R or other composite beams as shown in Fig.12b,c. This indicates that encasing the UHPFRC plates directly into the concrete flange, secured by reinforcement bars, effectively prevented any separation between the two surfaces until the complete failure of the composite beam. Additionally, the S2-R composite beam failed due to ductile flexural failure and rupture of the UHPFRC plates, indicating that all materials in the S2-R beam were fully utilized, whereas the S1-R composite beam failed due to shear with significant detachment at the interface beneath the flange occurred at peak load. The load-carrying and deformation capacities of S1-R and S2-R increased by 70.23% and 110.41%, and 45.79% and 381.31%, respectively, compared to the reference beam S0.

4.5. Effects of Interfacial Properties

By comparing the load vs mid-span deflection curves of specimens S2-R, S3-S, and S4-SC, as illustrated in Fig. 13, the effect of interfacial properties can be evaluated. The interfacial properties (rough, smooth, and smooth with steel connectors) significantly influenced shear-carrying capacities, as depicted in Fig. 14(a). The S2-R beam, which featured a rough interface, presented the greatest peak load and mid-span deflection, owing to its transition from brittle shear failure to ductile flexural failure. The superior performance of the S2-R beam can be attributed to the activation of multiple, redundant shear-transfer mechanisms. While the rough interface provided a baseline of shear resistance through friction and mechanical interlock, its primary contribution was likely in ensuring initial composite action. The critical component was the embedment of the UHPFRC plates into the flange, secured by the transverse reinforcement. These transverse bars acted as dowel connectors, providing a robust mechanical anchor that physically prevented vertical and horizontal slip at the interface. This mechanical anchorage carried the majority of the interfacial shear stress once micro-cracking began, preventing the progressive debonding observed in the S1-R beam. This robust connection maintained the integrity of the composite

section, allowing for significant stress redistribution. It forced the failure to occur within the materials themselves—yielding of the steel and crushing of the concrete—rather than at the weaker interface, thus enabling the transition from a brittle interface failure to a ductile flexural failure. The S3-S and S4-SC beams, with smooth and smooth with steel connectors interfaces, respectively, behaved similarly, indicating that, in comparison to the smooth interface, the steel connectors inserted in the UHPFRC plate did not considerably improve the interfacial bond. The load-carrying capacities of S2-R, S3-S, and S4-SC increased by 110.41%, 72.02%, and 76.19%, respectively, compared to the reference beam S0. As shown in Fig. 16(b), the deformation capacities at the peak load increased by 381.31%, 43.15%, and 40.50% for the respective beams. The smaller mid-span deflection in the S4-SC beam is attributed to the shear transfer mechanism facilitated by the steel connectors.

4.6. Effects of Core Concrete Type

To evaluate the impact of core concrete type on shear behavior, one beam (S5-HB) was constructed using cellular lightweight concrete (CLC) blocks instead of normal weight concrete (NWC). The S5-HB beam exhibited similar behavior to the composite beams S3-S and S4-SC, with approximately 34% less ductility, but the core weight was reduced by 72%. The reduced ductility of the S5-HB beam can be attributed to the significant stiffness mismatch between the low-modulus CLC core ($E \approx 2.1$ GPa) and the high-modulus UHPFRC shell ($E \approx 47$ GPa). This incompatibility likely led to strain concentrations at the interface, causing earlier micro-cracking and a more brittle failure of the core material compared to the NWC core beams. The shear and deformation capacities of S5-HB increased by 75% and 27.41%, respectively, compared to the reference beam S0. Overall, using CLC blocks instead of NWC for the core proves to be an effective, economical, and appropriate approach when reducing the structure's dead weight or thermal and sound insulation is a priority, but designers must account for the reduced shear capacity. However, it is important to note that the S5-HB specimen differed from the other beams in both its core material and its longitudinal reinforcement configuration. Therefore, the observed behavior reflects the combined effect of these changes, and the influence of the CLC core alone cannot be fully isolated in this study. This limitation should be considered when interpreting these results. Future research should investigate composite beams with CLC cores using an identical reinforcement layout to the NWC reference beam to directly quantify the effect of the core material. The choice of core material should be based on the specific design requirements and the desired balance between strength, stiffness, and weight.

4.7 Broader Implications and Practical Context

From a sustainability perspective, the composite approach offers significant material savings. For instance, for the beam cross-section studied, replacing the outer 30 mm shell with a UHPFRC plate reduces the required volume of normal weight concrete in the web by over 40%. This directly lowers cement consumption and the associated embodied carbon, highlighting the system's environmental benefits. Compared to other strengthening techniques like externally bonded CFRP, the proposed method offers the advantages of being a permanent formwork, which simplifies construction, and providing enhanced durability and impact resistance due to the UHPFRC shell. However, it is primarily suited for new constructions, whereas CFRP jacketing is more adaptable for retrofitting existing structures.

5. Conclusions

This research investigated the shear behavior of composite RC beams without stirrups, utilizing prefabricated UHPFRC plates as permanent formwork. The experimental program was limited to six beams and specific material combinations. Further testing with a larger sample size and different materials is recommended. Based on the experimental results, the following conclusions can be drawn:

- The use of prefabricated U-shaped UHPFRC plates as permanent formwork significantly enhanced the shear performance of RC beams without stirrups. Shear strength was increased

by 70.2% to 110.4%, and deformation capacity was increased by 27.4% to 381.3% compared to a conventional RC beam.

- Embedding the UHPFRC plates into the concrete flange, combined with a rough interface (beam S2-R), was the most effective configuration. It successfully transformed the failure mode from brittle shear to ductile flexure by preventing premature debonding and ensuring full composite action.
- Using a lightweight CLC block core reduced beam weight by 72% while still achieving a 75% increase in shear strength, demonstrating a viable trade-off between weight reduction and structural capacity.
- The findings suggest that this composite system is a promising solution for durable and efficient new concrete structures, particularly for achieving longer spans or shallower beam depths.

These conclusions are based on a limited set of six beams. To generalize the findings, further research with a broader scope is recommended. Future work should include a broader parametric study investigating the effects of UHPFRC plate thickness, different concrete core strengths (including higher-strength CLC), and varying shear span-to-depth ratios. Future work should also include long-term studies on durability and creep/shrinkage behavior. Complementing this research with validated finite element models would provide deeper insights for practical design and application.

References

[1] Monteagudo SM, Morán L, Vítores RP, González MS. The use of recycled materials in concrete. Construction and Building Materials. 2014;53:231-237. https://doi.org/10.1016/j.conbuildmat.2013.11.096

[2] Ghafari E, Costa H, Júlio E, Portugal A, Durães L. Enhanced durability of ultra high-performance concrete by incorporating supplementary cementitious materials. In: Proceedings of the Second International Conference on Microstructural-related Durability of Cementitious Composites; 2012; Amsterdam, The Netherlands.

[3] Ghafari E, Ghahari SA, Costa H, Júlio E, Portugal A, Durães L. Effect of supplementary cementitious materials on autogenous shrinkage of ultra-high performance concrete. Construction and Building Materials. 2016;127:43-48. https://doi.org/10.1016/j.conbuildmat.2016.09.123

[4] Alkaysi M, El-Tawil S. Effects of variations in the mix constituents of ultra high performance concrete (UHPC) on cost and performance. Materials and Structures. 2016;49(10):4185-4200. https://doi.org/10.1617/s11527-015-0780-6

[5] Ghafari E, Arezoumandi M, Costa H, Júlio E. Influence of nano-silica addition on durability of UHPC. Construction and Building Materials. 2015;94:181-188. https://doi.org/10.1016/j.conbuildmat.2015.07.009

[6] Carmo R, Júlio E. New trends for reinforced concrete structures: Some results of exploratory studies. Infrastructures. 2017;2(4):17. https://doi.org/10.3390/infrastructures2040017

[7] Júlio EN, Branco FA, Silva VD, Lourenço JF. Influence of added concrete compressive strength on adhesion to an existing concrete substrate. Building and Environment. 2006;41(12):1934-1939. https://doi.org/10.1016/j.buildenv.2005.06.023

[8] Júlio ENBS, Branco FAB, Silva VD. Concrete-to-concrete bond strength-influence of the roughness of the substrate surface. Construction and Building Materials. 2004;18(9):675-681. https://doi.org/10.1016/j.conbuildmat.2004.04.023

[9] Santos PMD, Júlio ENBS, Silva VD. Correlation between concrete-to-concrete bond strength and the roughness of the substrate surface. Construction and Building Materials. 2007;21(8):1688-1695. https://doi.org/10.1016/j.conbuildmat.2006.05.044

[10] Martins R, Carmo RNF, Costa H, Júlio E, Cordeiro T, Almeida V. Interface role in composite RC beams with a light-weight concrete core and an ultra high-durability concrete skin. Engineering Structures. 2021;228:111524. https://doi.org/10.1016/j.engstruct.2020.111524

[11] Carmo RNF, Martins R, Gonçalves R, Costa H, Júlio E. Effect of the outer UHDC layer on shear and flexural behavior of RC beams produced with low binder concrete. Construction and Building Materials. 2023;368:130402. https://doi.org/10.1016/j.conbuildmat.2023.130402

[12] Wassermann R, Katz A, Bentur A. Minimum cement content requirements: a must or a myth? Materials and Structures. 2009;42(7):973-982. https://doi.org/10.1617/s11527-008-9436-0

[13] Proske T, Hainer S, Rezvani M, Graubner C. Eco-friendly concretes with reduced water and cement content-mix design principles and application in practice. Construction and Building Materials. 2014;67:413-421. https://doi.org/10.1016/j.conbuildmat.2013.12.066
[14] Martins R, Carmo RNF, Costa H, Júlio E. Flexural behavior of eco-efficient and ultra-high durability concrete beams. Construction and Building Materials. 2020;236:117546. https://doi.org/10.1016/j.conbuildmat.2019.117546
[15] Robalo K, Soldado E, Costa H, Carvalho L, Carmo R, Júlio E. Durability and time-dependent properties of low-cement concrete. Materials. 2020;13(16):3583. https://doi.org/10.3390/ma13163583
[16] Zhang R, Hu P, Zheng X, Cai L, Guo R, Wei D. Shear behavior of RC slender beams without stirrups by using precast U-shaped ECC permanent formwork. Construction and Building Materials. 2020;260:120430. https://doi.org/10.1016/j.conbuildmat.2020.120430
[17] Hibbitt, Karlsson and Sorensen Inc. ABAQUS Theory Manual, User Manual and Example Manual. Version 6.7. Providence (RI): SIMULIA; 2000.
[18] Abdelkhalek A, Sakr MA, Seleemah AA, Khalifa TM. Effect of type of masonry units on the mechanical properties of masonry panel walls. International Journal of Masonry Research and Innovation. 2023;8(4-5):479-508. https://doi.org/10.1504/IJMRI.2023.131836
[19] Association Française du Génie Civil (AFGC). Ultra high performance fibre-reinforced concretes: Recommendations. Revised ed. Paris (France): AFGC/SETRA; 2013.
[20] Sakr MA. Finite element modeling of debonding mechanisms in carbon fiber reinforced polymer-strengthened reinforced concrete continuous beams. Structural Concrete. 2018;19(1):1-11.
[21] Sakr M, Osama B. Modeling of ultra-high performance fiber reinforced concrete filled steel tube columns under eccentric loading. Periodica Polytechnica Civil Engineering. 2022;66(4):1045-1057. https://doi.org/10.3311/PPci.20593
[22] Sakr MA, El-Khoriby SR, Khalifa TM, Nagib MT. Modeling of RC shear walls strengthened with ultra-high performance fiber reinforced concrete (UHPFRC) jackets. Engineering Structures. 2020;200:109696. https://doi.org/10.1016/j.engstruct.2019.109696
[23] Sakr MA, Osama B, El Korany TM. Modeling of ultra-high performance fiber reinforced concrete columns under eccentric loading. Structures. 2021;32:2195-2210. https://doi.org/10.1016/j.istruc.2021.04.026
[24] Sakr M, Sleemah A, Khalifa T, Mansour W. Shear strengthening of RC beams using prefabricated ultra-high performance fiber reinforced concrete (UHPFRC) plates: Experimental and numerical investigation. Structural Concrete. 2019;20(3):1137-1153. https://doi.org/10.1002/suco.201800137
[25] Saad AG, Sakr MA, El-Korany TM. The shear strength of existing non-seismic RC beam-column joints strengthened with CFRP sheets: Numerical and analytical study. Engineering Structures. 2023;291:116497. https://doi.org/10.1016/j.engstruct.2023.116497
[26] ASTM C1609/C1609M-19a. Standard test method for flexural performance of fiber-reinforced concrete (using beam with third-point loading). West Conshohocken (PA): ASTM International; 2019.
[27] BS EN 12390-3:2019. Testing hardened concrete - Part 3: Compressive strength of test specimens. London (UK): BSI Standards Publication; 2019.
[28] ASTM C39/C39M-21. Standard test method for compressive strength of cylindrical concrete specimens. West Conshohocken (PA): ASTM International; 2021.
[29] ACI Committee 544. Guide to design with fiber-reinforced concrete (ACI 544.4R-18). Farmington Hills (MI): American Concrete Institute; 2018.
[30] RILEM TC 162-TDF. Test and design methods for steel fibre reinforced concrete: Uniaxial tension test for steel fibre reinforced concrete. Materials and Structures. 2001;34(1):3-6. https://doi.org/10.1007/BF02482193
[31] Li V, He T. Shear behavior of composite beams with prefabricated UHPFRC formwork and lightweight aggregate concrete core without stirrups. Journal of Building Engineering. 2024;85:108520.
[32] Chen Y, Liu Z, Yu J. Shear performance of stirrup-free T-beams with a hybrid UHPFRC-NC web and a UHPFRC bottom flange. Engineering Structures. 2023;293:116664.
[33] Fang H, Zhao G, Huang L. Experimental and numerical study on shear behavior of RC beams strengthened with prefabricated UHPFRC panels with embedded connectors. Case Studies in Construction Materials. 2023;18:e02202. https://doi.org/10.1016/j.cscm.2023.e01860
[34] Al-Jaberi FKH, Al-Zuhairi AH. Shear behavior of reinforced concrete deep beams strengthened by using ultra-high performance fiber reinforced concrete layers. Research on Engineering Structures and Materials. 2024;10(1):163-178.
[35] ACI Committee 437. Code requirements for load testing of existing concrete structures and commentary (ACI 437.2-13). Farmington Hills (MI): American Concrete Institute; 2013.
[36] Lee JY, Kim SW. Shear behavior of reinforced concrete beams strengthened with wire-roped ultra-high performance fiber-reinforced concrete jackets. Composites Part B: Engineering. 2015;78:1-13.